Alkyne Adducts of $[W_2(OCH_2{}^tBu)_8]$. Cases of Perpendicular and Skewed Bridges in Equilibrium with Terminal Bonded Isomers

Malcolm H. Chisholm,*,† Damon R. Click,† Judith C. Gallucci,† Christopher M. Hadad,† and Paul J. Wilson‡

Department of Chemistry, The Ohio State University, 100 W. 18th Avenue, Columbus, Ohio 43210-1185, and Department of Chemistry, University of Bath, Claverton Down, Bath BA2 7AY, U.K.

Received June 27, 2003

Alkynes react with a suspension of $[W_2(OCH_2{}^tBu)_8](M{\equiv}M)$ in hydrocarbon solvents to give alkyne adducts $W_2(\mu\text{-}RCCR')(OCH_2{}^tBu)_8$, where R = H and R′ = Ph, Me, Me_3Si and R = Me and R′ = Me and Ph. For PhC≡CH, there is a μ-perpendicular mode of alkyne bonding, θ = 84°, but for MeC≡CH and MeC≡CMe, the bridging alkyne is distinctly skewed with respect to the W−W axis, θ = 64° and 67°, respectively. In contrast, the PhC≡CMe adduct has the alkyne bonded to only one tungsten, η^2-PhC≡CMe, with the alkyne C≡C axis being 30° from the W−W axis. In all of these structures, there are alkoxide bridges, and the dinuclear unit may be viewed as a confacial bioctahedron where either one alkyne and two alkoxides or three alkoxides occupy the bridging face. In toluene-d_8, NMR spectroscopic studies indicate that certain of these alkyne adducts (MeC≡CH, MeC≡CMe, PhC≡CMe, and $Me_3SiC{\equiv}CH$) exist as a mixture of alkyne-bridged and η^2-alkyne-bonded isomers. The isomers are fluxional on the NMR time scale by rapid exchange of terminal and bridging alkoxide groups. However, μ-η^2 alkyne exchange is slow on the NMR time scale. The structural data are compared with electronic structure calculations employing density functional theory on model compounds of formula W_2(alkyne)$(OMe)_8$. The calculations suggest that a μ-parallel mode of bonding is energetically favorable relative to μ-perpendicular and, further, that the energy difference between bridge and terminal alkyne adducts is, in all cases, less than 5 kcal mol^{-1}.

Introduction

In 1959, Sly reported the molecular structure of $Co_2(CO)_6(\mu$-PhC≡CPh), and in describing the cross-wise mode of alkyne addition to the dicobalt center, he noted that the mode of bonding bore correlation to that proposed for an alkyne on a metal surface.[1] This historic structure and Sly's prophetic comments concerning the bonding of alkynes to closely spaced metal centers heralded the advent of a golden era in organometallic cluster chemistry wherein relationships between organic fragments bonded to clusters (two or more metal centers) and those to surfaces were often cited.[2,3] There are now numerous examples of alkynes bridging to two, three, and four metal centers in discrete cluster compounds, and bridging modes of bonding are more common than terminal coordination as indeed they are for alkyne bonding to metal surfaces.[2,3] In 1982, Hoffmann, Hoffman, and Fisel noted that when alkynes bridge two metal atoms, they do so in a perpendicular or parallel manner, as exemplified by $Co_2(CO)_6(\mu$-PhC≡CPh)[1] and $Os_2(CO)_8(\mu$-RC≡CR).[4] In a limiting description, these may be termed as dimetalatetrahedranes and dimetallocyclobutadienes as shown in **A** and **B** below.[5]

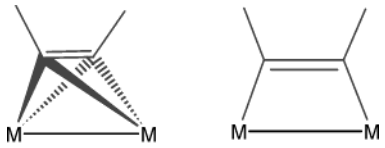

A **B**

† The Ohio State University.
‡ University of Bath.

(1) Sly, W. G. *J. Am. Chem. Soc.* **1959**, *81*, 18−20.

(2) (a) Thomas, J. M.; Thomas, W. J. *Principles and Practice of Heterogeneous Catalysis*; VCH: Weinheim, Germany, 1997. (b) Cox, P. A. *Transition Metal Oxides: An Introduction to their Electronic Structure and Properties*; Oxford University Press: New York, 1992. (c) Gates, B. *Catalytic Chemistry*; Wiley: New York, 1992. (d) *Mechanisms of Reactions of Organometallic Compounds with Surfaces*; Cole-Hamilton, D. J., Williams, J. O., Eds.; Plenum: New York, 1989. (e) Kung, H. H. *Transition Metal Oxides: Surface Chemistry and Catalysis*; Elsevier: Amsterdam, The Netherlands, 1989. (f) Kiselev, V. F.; Krylov, O. V. *Adsorption and Catalysis on Transition Metals and Their Oxides*; Springer: Heidelberg, Germany, 1989. (g) Hoffmann, R. *Solid and Surfaces, A Chemist's View of Bonding in Extended Strucures*; VCH: Weinheim, Germany, 1988. (h) Campbell, I. M. *Catalysis at Surfaces*; Chapman & Hall: London, U.K., 1988. (i) *Catalyst Design, Progress and Perspectives*; Hegedus, L., Ed.; Wiley: New York, 1987. (j) Bond, G. C. *Heterogeneous Catalysis, Principles and Applications*, 2nd ed.; Oxford University Press: New York, 1987. (k) Alberts, M. R.; Yates, J. T., Jr.. *The Surface Scientists Guide to Organometallic Chemistry*; American Chemical Society: Washington, D.C., 1987.

10.1021/om030498o CCC: $25.00
Publication on Web 10/18/2003

Since that time, a number of exceptions to the perpendicular or parallel modes of addition have been noted, and in each case the distortion from an idealized **A** or **B** type bonding mode has been traced to the existence of a second-order Jahn−Teller distortion.[6] This report details the continuing studies of the chemistry associated with the W═W bond in $[W_2(OCH_2{}^tBu)_8]_n$, in which we have found, for the first time, an equilibrium involving bridging and terminal bonding modes for 1:1 alkyne adducts. Diagrammatically, these can be represented as face-sharing octahedral complexes of the type shown in **C** and **D** where the alkyne occupies a single coordination site. Moreover, we show for each isomer that there is a low rotational barrier. A preliminary account of this work has appeared.[7]

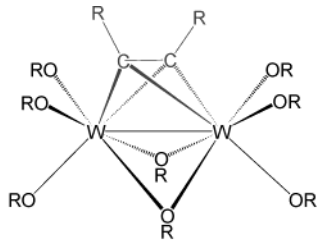

C

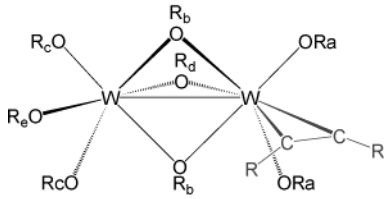

D

Results and Discussion

Preparation of Alkyne Adducts. Hydrocarbon suspensions of $[W_2(OCH_2Bu^t)_8]$ react with alkynes at room temperature or 45 °C to form the 1:1 adducts $W_2(OCH_2{}^tBu)_8(RC{\equiv}CR')$, where R = H and R′ = Me, Ph, or Me_3Si, and R = Me and R′ = Me or Ph. The preparation of the ethyne adduct (R = R′ = H) was noted earlier.[8] More complex chemistry was observed in related reactions involving ^{t}BuC≡CH and PhC≡CPh, and no simple 1:1 adduct was isolable. We do not speculate further on the latter reactions at this time.

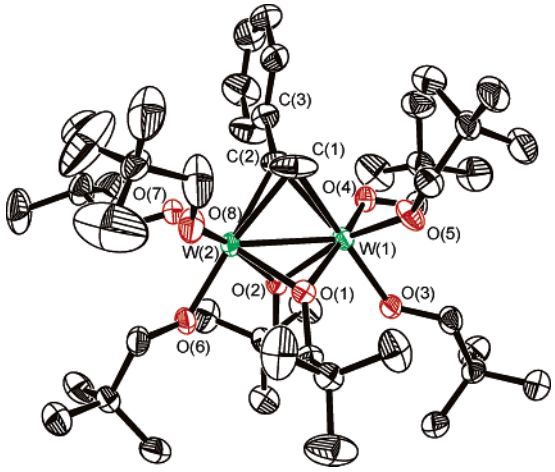

Figure 1. ORTEP[10] drawing of the molecular structure of $W_2(\mu\text{-}\eta^2,\eta^2\text{-}PhC{\equiv}CH)(\mu\text{-}OCH_2{}^tBu)_2(OCH_2{}^tBu)_6$, with thermal ellipsoids drawn at the 50% probability level.

The new 1:1 alkyne adducts form dark green solutions in hydrocarbon solvents, and dark crystalline samples suitable for X-ray studies were obtained from ether solutions upon cooling (−20 °C) and upon slow evaporation. All of the compounds are air-sensitive and must be handled in dry and oxygen-free atmospheres and solvents. The addition of the alkyne is known to be irreversible, as alkyne for alkyne′ exchange is not observed in solution, and the alkyne loss does not occur upon applying a dynamic vacuum to a solution of the 1:1 adducts. In contrast to the chemistry of 1:1 alkyne adducts of $W_2(OR)_6$ compounds (R = ^{t}Bu, ^{i}Pr, $CH_2{}^tBu$), no alkyne scission or alkyne C−C coupling reactions are observed.[9]

Single-Crystal and Molecular Structures. In this work, we have examined the structures of four compounds. The phenylacetylene adduct was found to have a μ-perpendicular alkyne bridge with a C−C/W−W twist angle of 84° (see Figure 1). In contrast, the propyne adduct and the dimethylacetylene adduct, Figures 2 and 3, have distinct nonperpendicular bridged structures with C−C/W−W twist angles of 64° and 67°, respectively. The solid-state structure of the phenylmethyl acetylene adduct is shown in Figure 4 and clearly has a η^2-mode of alkyne−tungsten bonding. Both of these structural types can be viewed as derivatives of confacial bioctahedra where one site is occupied by the alkyne C_2 moiety. (See **A** and **B** noted earlier.)

Selected bond distances and bond angles for these molecules are given in Tables 1 through 4. The W−W distances span a small range of 2.59−2.65 Å, and that for the η^2-PhC≡CMe adduct is not significantly different from that for the MeC≡CMe adduct. This distance is also very similar to that seen in alkyne adducts of

(3) (a) Corker, J.; Lefebvre, F.; Lecuyer, C.; Dufaud, V.; Quignard, F.; Choplin, A.; Evans, J.; Basset, J.-M. *Science* **1996**, *271*, 966. (b) Niccolai, G. P.; Basset, J.-M. *Appl. Catal., A* **1996**, *146*, 145. (c) Vidal, V.; Theolier, A.; Thivolle-Cazat, J.; Basset, J.-M.; Corker, J. *J. Am. Chem. Soc.* **1996**, *118*, 4595. For alkynes bound to clusters see: (d) Rosenberg, E.; Freeman, W.; Zinnia, C.; Hardcaastle, K.; Yoo, Y. J.; Milone, L.; Gobetto, R. *J. Cluster Sci.* **1992**, *3*, 439−57. (e) Deeming, A. J.; Arce, A. J.; DeSanctis, Y. *Mater. Chem. Phys.* **1991**, *29*, 323−31. (f) Shinsaku, Y. *Rec. Res. Dev. Pure Appl. Chem.* **1998**, *2*, 401−426. (g) Deabate, S.; Giordano, R.; Sappa, E. *J. Cluster Sci.* **1997**, *8*, 407−460. For a theoretical discussion of alkynes bound to metal surfaces see also: Silvestre, J.; Hoffmann, R. *Langmuir* **1985**, *1*, 621−647.

(4) (a) Burke, M. R.; Takats, J. *J. Organomet. Chem.* **1986**, *302*, C25. See also: (b) Grevels, F. H.; Klotzbuckner, W. E.; Seils, F.; Schaffner, K.; Takats, J. *J. Am. Chem. Soc.* **1990**, *112*, 1995. (c) Takats, J. *Polyhedron* **1988**, *7*, 931. (d) Bullock, R. M.; Hembre, R. T.; Norton, J. R. *J. Am. Chem. Soc.* **1988**, *110*, 0, 7868. (e) Hembre, R. T.; Scott, C. P.; Norton, J. R. *J. Am. Chem. Soc.* **1987**, *109*, 3468.

(5) Hoffman, D. M.; Hoffmann, R.; Fisel, C. R. *J. Am. Chem. Soc.* **1982**, *104*, 3858−75.

(6) (a) Chisholm, M. H.; Lynn, M. A. *J. Organomet. Chem.* **1998**, *550*, 141−150. (b) Cotton, F. A.; Feng, X. *Inorg. Chem.* **1990**, *29*, 3187−92. (c) Calhorda, M. J.; Hoffmann, R. *Organometallics* **1986**, *5*, 2181−7.

(7) Chisholm, M. H.; Click, D. R.; Gallucci, J. C.; Hadad, C. M.; Wilson, P. J. *J. Am. Chem. Soc.* **2002**, *124*, 14518.

(8) (a) Chisholm, M. H.; Folting, K.; Lynn, M. A.; Streib, W. E.; Tiedtke, D. B. *Angew. Chem., Int. Ed. Engl.* **1997**, *37*, 52. (b) Chisholm, M. H.; Streib, W. E.; Tiedtke, D. B. Wu, D.-D. *Chem. Eur. J.* **1998**, *4*, 1470.

(9) Chisholm, M. H.; Conroy, B. K.; Eichorn, B. W.; Folting, K.; Hoffman, D. M.; Huffman, J. C.; Marchant, N. S. *Polyhedron* **1987**, *6*, 783−792. For Mo see: Chisholm, M. H.; Hoffman, D. M.; McCandless Northius J.; Huffman, J. C. *Polyhedron* **1997**, *16*, 839−847.

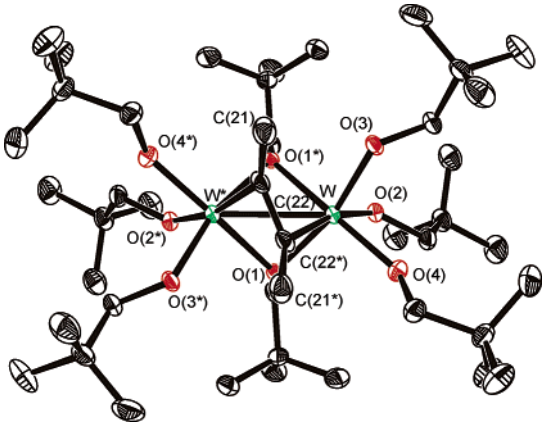

Figure 2. ORTEP[10] drawing of the molecular structure of $W_2(\mu\text{-}\eta^2,\eta^2\text{-MeC}{\equiv}\text{CMe})(\mu\text{-OCH}_2{}^t\text{Bu})_2(\text{OCH}_2{}^t\text{Bu})_6$, with thermal ellipsoids drawn at the 50% probability level. * indicates the following symmetry transformation: $-x + 1$, y, $-z + 1/2$.

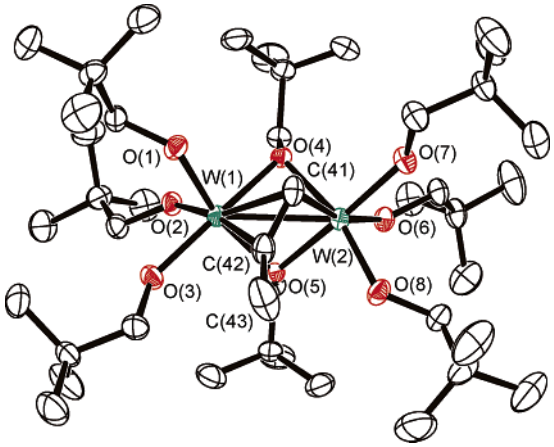

Figure 3. ORTEP[10] drawing of the molecular structure of $W_2(\mu\text{-}\eta^2,\eta^2\text{-MeC}{\equiv}\text{CH})(\mu\text{-OCH}_2{}^t\text{Bu})_2(\text{OCH}_2{}^t\text{Bu})_6$, with thermal ellipsoids drawn at the 50% probability level.

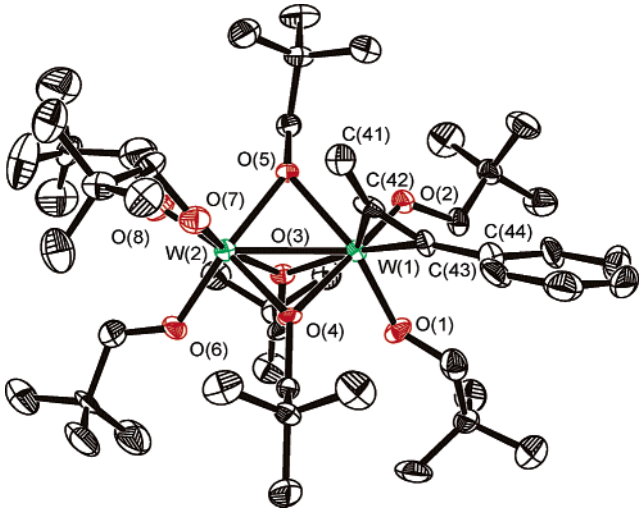

Figure 4. ORTEP[10] drawing of the molecular structure of $W_2(\eta^2\text{-PhC}{\equiv}\text{CMe})(\mu\text{-OCH}_2{}^t\text{Bu})_3(\text{OCH}_2{}^t\text{Bu})_5$, with thermal ellipsoids drawn at the 50% probability level.

$W_2(OR)_6$ compounds, where additional pyridine (py) ligands are also present, e.g., $W_2(O^tBu)_6(\mu\text{-HCCH})(py)$ and $W_2(O^iPr)_6(\mu\text{-MeC}{\equiv}\text{CMe})(py)_2$.[8] However, the C−C distances in the latter are notably longer, *ca.* 1.4 Å versus ca. 1.3 Å in the present work. This can be attributed to the greater reducing power of the $(W{\equiv}W)^{6+}$ center relative to $(W{=}W)^{8+}$. However, the fact that the C−C−C angles for both the μ- and η^2-adducts fall in the range of 126° (MeC≡CMe) to 136° and 141° (PhC≡CMe), respectively, clearly implies extensive W d_π to alkyne π^* back-bonding, irrespective of the mode of addition. The W−O distances reveal the expected trend with W−μ-O being longer than the W−O terminal and also reveal that the W−O distances trans to the alkyne, be they bridging or terminal, are longer than W−O distances which are mutually trans. Thus the alkyne exerts a higher trans-influence than the W−OR bonds. In the case of the η^2-PhC≡CMe adduct, the alkyne C≡C axis is rotated ∼30° from collinearity with the W−W axis. The W−C distances in the η^2-alkyne adduct are comparable to the short W−C bridging distances in the nonperpendicular bridged adducts (MeC≡CMe and MeC≡CH). Furthermore, each metal center can formally be regarded as having different oxidation states. If oxidation states are assigned in the manner −2 for the alkyne and −1 for the terminal alkoxides and $-^1/_2$ for the bridging alkoxides, then W(1) is in the oxidation state $+4^1/_2$ and W(2) is in the oxidation state $+5^1/_2$.

Table 1. Selected Bond Distances (Å) and Angles (deg) for $W_2(\mu\text{-}\eta^2,\eta^2\text{-PhC}{\equiv}\text{CH})(\mu\text{-OCH}_2{}^t\text{Bu})_2(\text{OCH}_2{}^t\text{Bu})_6$ and Those Calculated for the Model Complex $W_2(\mu\text{-}\eta^2,\eta^2\text{-PhC}{\equiv}\text{CH})(\mu\text{-OCH}_3)_2(\text{OCH}_3)_6$

bond		distance	bond		distance
W(1)−W(2)	expt	2.5957(2)	W(2)−O(1)	expt	2.124(2)
	calc	2.70		calc	2.12
W(1)−O(1)	expt	2.105(2)	W(2)−O(2)	expt	2.088(2)
	calc	2.15		calc	2.13
W(1)−O(2)	expt	2.088(2)	W(2)−O(6)	expt	1.975(2)
	calc	2.10		calc	1.98
W(1)−O(3)	expt	1.959(2)	W(2)−O(7)	expt	1.911(2)
	calc	1.98		calc	1.94
W(1)−O(4)	expt	1.893(2)	W(2)−O(8)	expt	1.886(2)
	calc	1.89		calc	1.92
W(1)−O(5)	expt	1.892(2)	W(2)−C(1)	expt	2.259(4)
	calc	1.95		calc	2.49
W(1)−C(1)	expt	2.195(4)	W(2)−C(2)	expt	2.237(4)
	calc	2.10		calc	2.13
W(1)−C(2)	expt	2.320(3)	C(1)−C(2)	expt	1.251(5)
	calc	2.32		calc	1.26

bond		angle	bond		angle
W(1)−O(1)−W(2)	expt	75.63(7)	O(1)−W(1)-O(4)	expt	165.8(1)
	calc	78.40		calc	166.2
W(1)−O(2)−W(2)	expt	76.77(7)	O(1)−W(2)-O(7)	expt	169.0(1)
	calc	79.12		calc	157.2
W(1)−C(2)−W(2)	expt	69.3(1)	O(2)−W(1)-O(5)	expt	164.9(1)
	calc	66.3		calc	160.5
W(1)−C(1)−W(2)	expt	71.2(1)	O(2)−W(2)-O(8)	expt	165.0(1)
	calc	71.5		calc	170.3
C(1)−C(2)−C(3)	expt	138.1(4)			
	calc	128.0			

Solution NMR Behavior. All of the new compounds reported display rather complex NMR spectra that are temperature dependent and in most instances reflect the presence of two isomers in solution that show fluxional properties. Selected ^{1}H NMR spectra for the PhC≡CH adduct are shown in Figure 5.

The low-temperature spectrum is consistent with the major isomer in solution being the bridged alkyne adduct (>90%), which adopts a time-averaged mirror symmetry leading to ^{t}Bu resonances that fall in the ratio 1:1:2:2:2. Moreover, the methylene protons associated with the two bridging alkoxides lie on the mirror plane

Table 2. Selected Bond Distances (Å) and Angles (deg) for $W_2(\mu\text{-MeC}{\equiv}\text{CMe})(\mu\text{-OCH}_2{}^t\text{Bu})_2(\text{OCH}_2{}^t\text{Bu})_6$ Compared with Those Calculated for the Model Compound $W_2(\mu\text{-MeC}{\equiv}\text{CMe})(\mu\text{-OCH}_3)_2(\text{OCH}_3)_6$

bond		distance	bond		distance
W(*)−W(2)	expt	2.6361(2)	W(*)−O(3*)	expt	1.890(2)
	calc	2.66		calc	1.91
W(*)−C(22)	expt	2.085(3)	W(*)−O(4*)	expt	1.913(2)
	calc	2.12		calc	1.94
W(*)−C(22*)	expt	2.396(3)	C(22)−C(22*)	expt	1.354(5)
	calc	2.52		calc	1.36
W(*)−O(1)	expt	2.065(1)	W(*)−O(2*)	expt	1.959(2)
	calc	2.12		calc	2.00
W(*)−O(1*)	expt	2.134(2)			
	calc	2.13			

bond		angle	bond		angle
W(*)−C(22)−W	expt	71.69(9)	O(2)−W−C(22*)	expt	166.1(1)
	calc	69.18		calc	168.8
W(*)−O(1*)−W	expt	77.77(6)	O(2)−W−C(22)	expt	158.1(1)
	calc	77.76		calc	158.9
O(1*)−W−O(4)	expt	165.43(8)	C(22*)−C(22)−C(21)	expt	126.3(2)
	calc	157.00		calc avg.	128.7
O(1)−W−O(3)	expt	165.76(7)	O(1*)−W(*)−O(3*)	calc	169.29
	calc	169.29	O(1)−W(*)−O(4*)	calc	156.87

Table 3. Selected Bond Distances (Å) and Angles (deg) for $W_2(\mu\text{-}\eta^2,\eta^2\text{-MeC}{\equiv}\text{CH})(\mu\text{-OCH}_2{}^t\text{Bu})_2(\text{OCH}_2{}^t\text{Bu})_6$ and a Comparison with Those Calculated for the Model Complex $W_2(\mu\text{-MeC}{\equiv}\text{CH})((\mu\text{-OCH}_3)_2(\text{OCH}_3)_6$

bond		distance	bond		distance
W(1)−W(2)	expt	2.6295(2)	W(2)−O(4)	expt	2.066(2)
	calc	2.68		calcd	2.13
W(1)−O(1)	expt	1.882(2)	W(2)−O(5)	expt	2.127(2)
	calc	1.94		calcd	2.12
W(1)−O(2)	expt	1.963(2)	W(2)−O(6)	expt	1.948(2)
	calc	2.00		calc	1.98
W(1)−O(3)	expt	1.918(2)	W(2)−O(7)	expt	1.924(2)
	calc	1.94		calc	1.94
W(1)−O(4)	expt	2.130(2)	W(2)−O(8)	expt	1.887(2)
	calc	2.13		calc	1.90
W(1)−O(5)	expt	2.075(2)	W(2)−C(41)	expt	2.057(3)
	calc	2.13		calc	2.10
W(1)−C(41)	expt	2.366(3)	W(2)−C(42)	expt	2.454(3)
	calc	2.47		calc	2.61
W(1)−C(42)	expt	2.088(3)	C(1)−C(2)	expt	1.332(4)
	calc	2.11		calc	1.35

bond		angle	bond		angle
W(1)−O(4)-W(2)	expt	77.57(6)	O(4)−W(1)−O(3)	expt	163.23(7)
	calc	78.08		calc	157.44
W(1)−O(5)−W(2)	expt	77.46(6)	O(4)−W(2)−O(8)	expt	165.51(8)
	calc	78.13		calc	166.34
W(1)−C(41)−W(2)	expt	72.57(9)	O(5)−W(2)−O(7)	expt	166.60(7)
	calc	71.28		calc	159.88
W(1)−C(42)−W(2)	expt	70.22(8)	O(5)−W(1)−O(1)	expt	166.82(7)
	calc	67.94		calc	168.74
C(41)−C(42)−C(43)	expt	127.0(3)			
	calc	129.5			

and thus appear as 1:1 singlets, whereas all other methylene protons are diastereotopic. The alkyne CH resonance appears downfield at ca. 12 ppm and is flanked by satellites (25%) due to coupling to ^{183}W, $I = {}^1/_2$, 14.5% natural abundance. From the relative intensities of the satellites, we can be sure that this proton is attached to a carbon atom that bridges two tungsten atoms in a time-averaged symmetrical manner. The ^{1}H NMR spectra of the PhC≡CH adduct are, in many ways, the easiest to reconcile with the solid-state molecular structure.

The ^{1}H NMR spectra of the TMSC≡CH adduct are shown in Figure 6, and at first glance, the room-temperature spectrum is deceptively similar to the low-temperature spectrum of the PhC≡CH adduct inasmuch as the major isomer (>95%) has mirror symmetry. The TMSC≡CH adduct is, however, frozen out on the NMR time scale at 25 °C, and the alkyne CH proton shows satellites (12.5%) due to coupling to ^{183}W, $I = {}^1/_2$, 14.5% natural abundance, and indicate that the CH carbon is bound to only one tungsten atom. Upon raising the temperature, the alkoxides undergo a selective exchange. This too is in contrast to the dynamic behavior of the PhC≡CH adduct, wherein all of the alkoxide ligands enter into site exchange. The NMR spectra for the TMSC≡CH adduct are reconcilable with a η^2-alkyne adduct similar to that seen in the solid-state molecular structure for the PhC≡CMe adduct. The variable-temperature dynamic NMR behavior may be explained by the selective bridge ⇌ terminal alkoxide exchange of the groups denoted R_b, R_c, R_d, and R_e in the schematic confacial bioctahedral drawing **D**. This can be under-

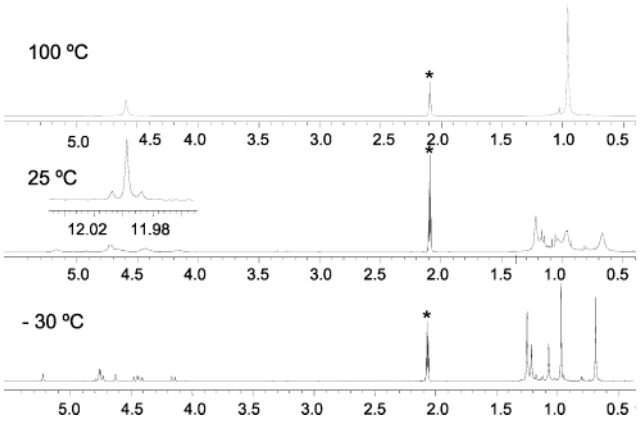

Figure 5. 400 MHz ^{1}H NMR spectra of $W_2(\mu\text{-}\eta^2,\eta^2\text{-PhC}\equiv\text{CH})(\mu\text{-OCH}_2{}^t\text{Bu})_2(\text{OCH}_2{}^t\text{Bu})_6$ at −30, 25, and 100 °C in toluene-d_8. * denotes protio impurity in toluene-d_8. The inset shown in the 25 °C spectrum shows the PhC≡C*H* proton signal flanked by satellites due to coupling to ^{183}W.

Table 4. Selected Bond Distances (Å) and Angles (deg) for $W_2(\eta^2\text{-PhC}\equiv\text{CMe})(\mu\text{-OCH}_2{}^t\text{Bu})_3(\text{OCH}_2{}^t\text{Bu})_5$ and a Comparison with Those Calculated for the Model Compound $W_2(\eta^2\text{-PhC}\equiv\text{CMe})(\mu\text{-OCH}_3)_3(\text{OCH}_3)_5$

bond		distance	bond		distance
W(1)−W(2)	expt	2.6536(5)	W(1)−C(43)	expt	2.081(9)
	calc	2.71		calc	2.08
W(1)−O(1)	expt	1.981(6)	W(2)−O(3)	expt	2.055(6)
	calc	1.99		calc	2.08
W(1)−O(2)	expt	1.922(6)	W(2)−O(4)	expt	2.062(5)
	calc	1.94		calc	2.08
W(1)−O(3)	expt	2.201(6)	W(2)−O(5	expt	2.069(6)
	calc	2.24		calc	2.09
W(1)−O(4	expt	2.115(6)	W(2)−O(6)	expt	1.919(6)
	calc	2.14		calc	1.95
W(1)−O(5)	expt	2.158(6)	W(2)−O(7)	expt	1.856(7)
	calc	2.20		calc	1.89
W(1)−C(42)	expt	2.057(9)	W(2)−O(8)	expt	1.914(6)
	calc	2.05		calc	1.94
C(42)−C(43)	expt	1.35(1)			
	calc	1.32			

bond		angle	bond		angle
W(1)−O(3)−W(2)	expt	77.0(2)	O(4)−W(2)−O(8)	expt	168.2(3)
	calc	77.6		calc	159.3
W(1)−O(4)−W(2)	expt	78.9(2)	O(5)−W(1)−O(1)	expt	151.9(3)
	calc	79.9		calc	149.7
W(1)−O(5)−W(2)	expt	77.7(2)	O(5)−W(2)−O(6)	expt	163.3(3)
	calc	78.2		calc	171.3
O(4)−W(1)-O(2)	expt	166.6(2)	O(3)−W(1)−C(43)	expt	169.5(3)
	calc	167.4		calc	136.8
C(41)−C(42)−C(43)	expt	140.6(9)	O(3)−W(1)−C(42)	expt	142.1(3)
	calc	140.2		calc	145.2
C(44)−C(43)−C(42)	expt	135.8(9)			
	calc	137.3			

stood to result from the high trans-influence of the η^2-alkyne. The long and presumably labile bridging W−OR_d bond breaks, leaving one tungsten atom six-coordinate (six W−O bonds) and the other five-coordinate. If we assume that each metal is now stereochemically labile, the re-formation of the alkoxide bridge bond will have scrambled R_d with R_e and R_c, which were terminal, and R_d with R_b, which was bridging. The other two terminal alkoxides, R_a, which are bonded to the tungsten center bearing the η^2-alkyne ligand are not involved in this exchange process. Alkoxide group identity was established by a NOE experiment, and connectivity was established by a NOESY experiment. (See Supporting Information.)

The propyne and 2-butyne adducts, which both adopt skewed bridged structures in the solid state, exist in solution as 3:1 and 1:9 bridged to terminal (**C** to **D**) structures, respectively. The NMR spectra of the 2-butyne adduct is further complicated by the fact that we observe alkyne−tungsten bond rotation for the η^2-alkyne ligand. (See Figure 7.) Although the bridged isomers are severely skewed in the solid-state molecular structures with W−C distances of 2.08 and 2.40 Å, we are not able to detect this behavior in solution. Most likely, this indicates that the barrier to oscillation about a symmetrical μ-perpendicular bridge is smaller than thermal energy.

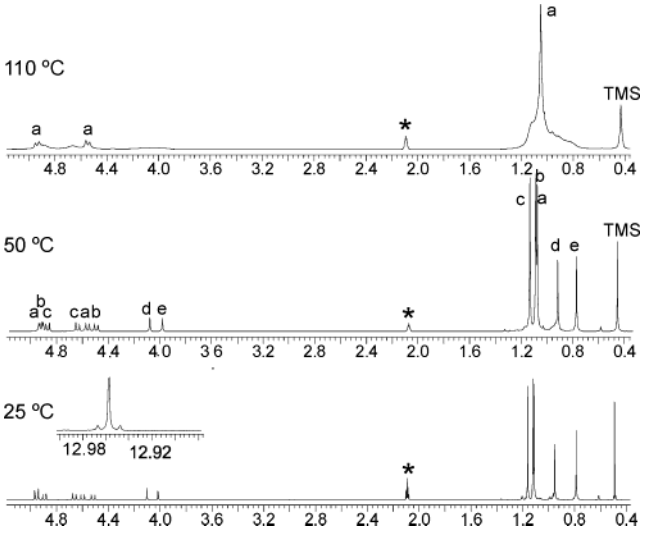

Figure 6. 400 MHz ^{1}H NMR spectra of $W_2(\eta^2\text{-TMSC}\equiv\text{CH})(\mu\text{-OCH}_2{}^t\text{Bu})_3(\text{OCH}_2{}^t\text{Bu})_5$ showing selective alkoxide group exchange upon warming from 25 to 110 °C. * denotes protio impurity in toluene-d_8. The inset to the 25 °C spectrum shows the TMSC≡C*H* resonance flanked by satellites due to coupling to ^{183}W.

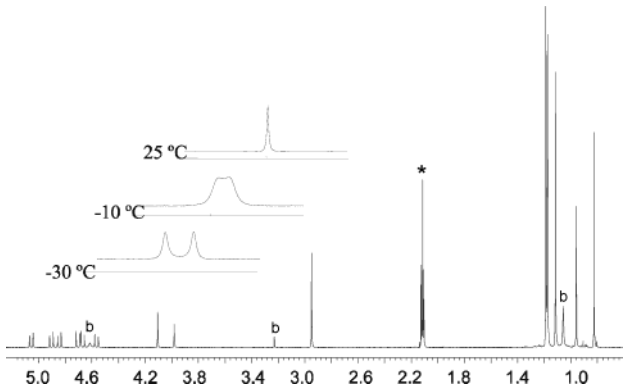

Figure 7. 400 MHz ^{1}H NMR spectra of the $W_2(\text{OCH}_2{}^t\text{Bu})_8(\text{MeC}\equiv\text{CMe})$ adduct at 25 °C. * denotes the protio impurity in tolune-d_8 and 'b' denotes the resonances for the bridging structure $W_2(\mu\text{-}\eta^2,\eta^2\text{-MeC}\equiv\text{CMe})(\mu\text{-OCH}_2{}^t\text{Bu})_2(\text{OCH}_2{}^t\text{Bu})$. The major isomer is $W_2(\eta^2\text{-MeC}\equiv\text{CMe})(\mu\text{-OCH}_2{}^t\text{Bu})_3(\text{OCH}_2{}^t\text{Bu})_5$ with the 2-butyne CH_3 resonance(s) at *ca.* 3.0 ppm shown in the inset at −30, −10, and 25 °C.

The ^{1}H NMR spectrum of the methylene protons of the neopentoxide ligands of the propyne adducts is shown in Figure 8. This dramatically reveals that the μ-alkyne adduct is fluxional but not exchanging with the η^2-alkyne adduct, which is not undergoing alkoxide group exchange on the NMR time scale at this temperature. Even at 100 °C in toluene-d_8, there is no NMR evidence for rapid exchange of the bridging and terminal

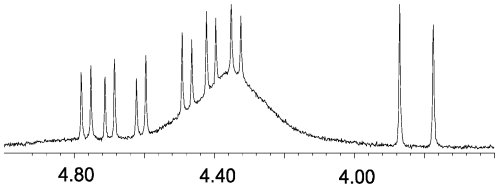

Figure 8. 400 MHz ^{1}H NMR spectrum of the methylene region for $W_2(\mu\text{-}\eta^2,\eta^2\text{-MeC}{\equiv}\text{CH})(\mu\text{-OCH}_2{}^t\text{Bu})_2(\text{OCH}_2{}^t\text{Bu})_6$ at 25 °C.

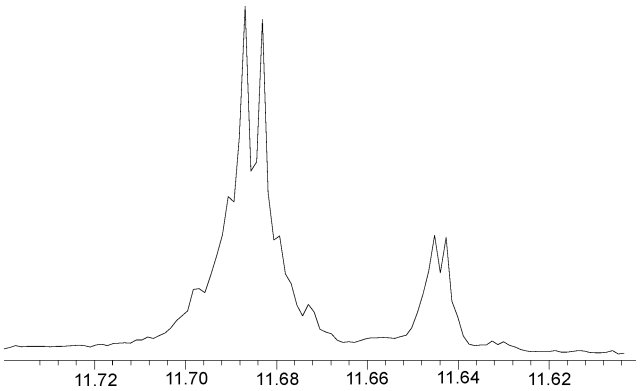

Figure 9. 400 MHZ ^{1}H NMR spectrum of the CH alkyne region of the propyne adducts at 25 °C.

alkyne adducts despite the fact that each isomer is fluxional.

The ^{1}H NMR spectrum of the CH alkyne region of the propyne adducts is shown in Figure 9. The alkyne resonances appear as quartets, due to long-range coupling with the methyl protons, and each are flanked by a pair of quartets due to coupling to ^{183}W. From the relative intensities of the flanking satellites, it is apparent that the alkyne proton of the downfield signal is attached to a carbon atom that bridges two tungsten atoms. The major isomer is the bridged form, **C**, while the minor isomer is the η^2-alkyne adduct, **D**.

The PhC≡CMe adduct, which is the only compound that we have characterized as a η^2-alkyne adduct of the type **D** in the solid state, exists in solution as a mixture of bridging and terminal isomers, **C** and **D**, in a 1:3 ratio and shows dynamic behavior akin to that described above. There is also another example of a dinuclear complex having a terminal bound alkyne, namely, $Cp^*(CO)_2Re(\mu\text{-CO})Re(CO)(\eta^2\text{-CH}_3C{\equiv}CCH_3)Cp^*$. However, this compound was seen only at low temperature by ^{1}H NMR (−78 °C), and upon warming above −20 °C, a metallocyclopentadienone was formed.[11]

Computational Studies: Bonding Considerations. The bonding in the ethyne adduct $W_2(\mu\text{-}\eta^2,\eta^2\text{-HC}{\equiv}\text{CH})(\mu\text{-OCH}_2{}^t\text{Bu})_2(\text{OCH}_2{}^t\text{Bu})_6$ has been examined previously by various computational methods [extended Huckel (EHMO), Fenske−Hall and RHF (restricted Hartree−Fock), and density functional theory (B3LYP)] on the model compound $W_2(\mu\text{-}\eta^2,\eta^2\text{-HC}{\equiv}\text{CH})(\mu\text{-OH})_2(\text{OH})_6$].[5a] The EHMO and Fenske−Hall calculations suggested that the lowest energy form should have a μ-parallel mode of bonding akin to that seen in $Os_2(CO)_8(\mu\text{-RC}{\equiv}\text{CR}')$ compounds, thus supporting the simple expectations based on the similarity of d^2-$W(OR)_4$ and d^8-$M(CO)_4$ fragment molecular orbitals. However, the RHF calculations reproduced the skewed-bridged structure seen in the solid state and supported the frontier molecular orbital expectations for a second-order Jahn−Teller distortion. The similarity between the electronic structure of $W_2(\mu\text{-}\eta^2,\eta^2\text{-HC}{\equiv}\text{CH})(\mu\text{-OH})_2(\text{OH})_6$ and $W_2(\mu\text{-}\eta^2,\eta^2\text{-HC}{\equiv}\text{CH})(\mu\text{-NH}_2)_2\text{Cl}_6^{2-}$ was also noted, which emphasized that the distortion has an electronic origin rather than a steric one.[5a] We shall not comment further on the bonding in the bridged isomers except to state that we have now employed DFT calculations[12,13] with the Gaussian 98 suite of programs[14] to calculate the minimum energy structures of the bridged alkyne adducts, $W_2(\mu\text{-}\eta^2,\eta^2\text{-RC}{\equiv}\text{CR})(\mu\text{-OCH}_3)_2(\text{OCH}_3)_6$, for the alkynes HC≡CH, MeC≡CH, PhC≡CH, TMSC≡CH, MeC≡CMe, and PhC≡CMe utilizing the B3LYP[15−17] method and standard basis sets. C, H, O, and Si were described with the 6-31G* basis set[18] (and five "pure" d functions), while W was represented by an SDD effective core potential.[19] All optimizations were carried out under C_1 symmetry starting from the crystal structure coordinates of either $W_2(\mu\text{-}\eta^2,\eta^2\text{-HC}{\equiv}\text{CH})(\mu\text{-OCH}_2{}^t\text{Bu})_2(\text{OCH}_2{}^t\text{Bu})_6$ (for HC≡CH and MeC≡CH), $W_2(\mu\text{-}\eta^2,\eta^2\text{-MeC}{\equiv}\text{CMe})(\mu\text{-OCH}_2{}^t\text{Bu})_2(\text{OCH}_2{}^t\text{Bu})_6$ (for MeC≡CMe, TMSC≡CH, and PhC≡CMe), or $W_2(\mu\text{-}\eta^2,\eta^2\text{-PhC}{\equiv}\text{CH})(\mu\text{-OCH}_2{}^t\text{Bu})_2(\text{OCH}_2{}^t\text{Bu})_6$ (for PhC≡CH). In all cases, a minimum energy structure was found, and all stationary points were characterized as minima by complete vibrational frequency calculations. Geometrical parameters for these six structures are all very similar and are given in the Supporting Information. Comparisons with experimentally observed μ-isomers are also given in Tables 1−3.

Attempted DFT calculations on μ-parallel bridged alkyne adducts (alkyne = HC≡CH, PhC≡CH, TMSC≡CH) indicated this bridging mode was lower in energy than the μ-perpendicular alkyne adducts, although the energy difference was small, ∼5−10 kcal/mol. We can conclude that the observed twist angle, θ, is largely determined by steric factors and that any barrier to μ-perpendicular ⇌ μ-parallel interconversion, i.e., alkyne rotation about the W_2 moiety, that could be monitored

(10) Johnson, C. K. *ORTEP II: Oak Ridge Thermal Ellipsoid Plot Program for Crystal Structure Illustrations*; Oak Ridge National Laboratory Report ORNL-5138; 1976.

(11) Casey, C. P.; Carino, R. S.; Hayashi, R. K. Schadesky, D. K. *J. Am. Chem. Soc.* **1996**, *118*, 1617. (b) Casey, C. P.; Carino, R. S.; Sakaba, H.; Hayashi, R. K. *Organometallics* **1996**, *15*, 2640−49. (c) Casey, C. P.; Carino, R. S.; Sakaba, H. *Organometallics* **1997**, *16*, 419−426. (d) Casey, C. P.; Carino, R. S.; Brady, J. T.; Hayashi, R. K. *J. Organomet. Chem.* **1998**, *569*, 55−60.

(12) Parr, R. G.; Yang, W. *Density-functional Theory of Atoms and Molecules*; Oxford University Press: New York, 1989.

(13) Labanowski, J. K.; Andzelm, J. W. Editors, *Density Functional Methods in Chemistry*; Springer-Verlag: Berlin, 1991.

(14) Frisch, M. J.; Trucks, G. W.; Schlegel, H. B.; Scuseria, G. E.; Robb, M. A.; Cheeseman, J. R.; Zakrzewski, V. G.; Montgomery, J. A. J.; Stratmann, R. E.; Burant, J. C.; Dapprich, S.; Millam, J. M.; Daniels, A. D.; Kudin, K. N.; Strain, M. C.; Farkas, O.; Tomasi, J.; Barone, V.; Cossi, M.; Cammi, R.; Menuucci, B.; Pomelli, C.; Adamo, C.; Clifford, S.; Ochterski, J.; Pertersson, G. A.; Ayala, P. Y.; Cui, Q.; Morokuma, K.; Malick, D. K.; Rabuck, A. D.; Raghavachari, K.; Foresman, J. B.; Cioslowski, J.; Ortiz, J. V.; Baboul, A. G.; Stefanov, B. B.; Liu, G.; Liashenko, A.; Piskorz, P.; Komaromi, I.; Gomperts, R. J.; Martin, R. L.; Fox, D. J.; Keith, T.; Al-Lahman, M. A.; Peng, C. Y.; Nanayakkara, A.; Challacombe, M.; Gill, P. M. W.; Johnson, B.; Chen, W.; Wong, M. W.; Andres, J. L.; Gonzalez, C.; Head-Gordon, M.; Replogle, E. S.; Pople, J. A. *Gaussian 98 Version A9*; Gaussian Inc.: Pittsburgh, PA, 1998.

(15) Becke, A. D. *Phys. Rev. A: Gen. Phys.* **1988**, *38*, 3098.

(16) Becke, A. D. *J. Chem. Phys.* **1993**, *98*, 5648.

(17) Lee, C.; Yang, W. R.; Parr, G. *Phys. Rev. B: Condens. Matter* **1988**, *37*, 785.

(18) Hehre, W. J.; Radom, L.; P.; Schleyer, P. v. R.; Pople J. A. *Ab Initio Molecular Orbital Theory*; John Wiley & Sons: New York, 1986.

(19) Andrae, D.; Haeussermann, U.; Dolg, M.; Stoll, H.; Preuss, H. *Theor. Chim. Acta* **1990**, *77*, 123.

Table 5. DFT Calculated Energy Differences between the μ- and η^2-alkyne Adducts of $W_2(OCH_3)_8$

	alkyne											
	HC≡CH		MeC≡CH		PhC≡CH		TMSC≡CH		MeC≡CMe		PhC≡CMe	
coordination	η-	μ-	η-	μ-	η-	μ-	η-	μ-	η-	μ-	η-	μ-
Δ (kcal/mol)	0	2.8	0	3.8	0	4.3	0	5.6	0	3.0	0	5.2

on the NMR time scale is largely determined by steric considerations.

The bonding in a related set of η^2-alkyne adducts of $W_2(OCH_3)_8$ was also investigated using DFT calculations starting with the coordinates taken from the observed solid-state molecular structure of the PhC≡CMe adduct. Again, the structures were fully optimized under C_1 symmetry, and vibrational frequency calculations were performed to verify each stationary point as a true minimum. A comparison of the calculated geometrical parameters for $W_2(\eta^2\text{-PhC}{\equiv}\text{CMe})(\mu\text{-OCH}_3)_2(\text{OCH}_3)_6$ with those observed for $W_2(\eta^2\text{-PhC}{\equiv}\text{CMe})(\mu\text{-OCH}_2{}^t\text{Bu})_2(\text{OCH}_2{}^t\text{Bu})_6$ is given in Table 4. A summary of the geometrical parameters for all six η^2-alkyne adducts is given in the Supporting Information.

On the basis of the total energy, we find that the μ- and η^2-alkyne adducts of $W_2(OCH_3)_8$ are predicted to be very similar in energy (see Table 5). In all cases, the η^2-alkyne adduct is predicted to be lower in energy by 2.8−5.2 kcal/mol. However, this small energy difference is similar to expected uncertainties based on the level of computation. What is perhaps rewarding, based on these calculations, is the expectation that the μ- and η^2-alkyne isomers can readily be expected to be in equilibrium. Moreover, given the complicated nature of the orbital interactions that occur for a confacial bioctahedral molecule with σ and π that are significantly influenced by M−O−C angles of the OCH_3 ligands, the calculated frontier molecular orbitals find some remarkable appeal to one's sense of what should be important in the bonding for an alkyne adduct of this type. Selected frontier molecular orbitals are shown in Figure 10.

The HOMO is clearly identifiable as a W−W σ-bonding molecular orbital arising from overlap of the metals' d_{z^2}−d_{z^2} orbitals. The HOMO-1 is comprised of a tungsten−carbon bonding MO that results from the W d_π to C_2 π^* back-bonding, and the HOMO-2 is alkyne C−C π bonding that is perpendicular to the W−C_2 axis and is not principally involved in bonding to the metal center. The HOMO-3 is an oxygen-based lone-pair combination, while the HOMO-4 is the C_2 π filled to W σ-bonding molecular orbital. The LUMO is a metal-based d orbital that is centered on the tungsten atom that forms six W−O bonds. It has δ symmetry with respect to the W−W axis but is not M−M bonding. In a simple-minded picture, the molecule can be viewed as a d^1-W−d^3-W-(η^2-alkyne) dimer within a confacial bioctahedral σ framework. Each metal uses one of the t_{2g} orbitals to form a M−M σ bond, and one metal has a t_{2g}−$C_2\pi^*$ orbital interaction. It is thus not surprising that alkyne rotation is observed on the NMR time scale for the η^2-alkyne adducts.

Conclusions

This work has provided the first examples of an equilibrium involving η^2- and μ-alkyne bonding to a dinuclear metal center. Moreover, each isomer form has been shown to be fluxional on the NMR time scale, although the equilibrium is rapid only on the chemical time scale. Evidently, in the compounds $W_2(\mu\text{-alkyne})(\mu\text{-OCH}_2{}^t\text{Bu})_2(\text{OCH}_2{}^t\text{Bu})_6$, the barrier for bridging alkyne ⇌ terminal alkyne site exchange is larger than that for alkoxide group exchange within each isomer. The calculations carried out on the $W_2(\text{alkyne})(OCH_3)_8$ template underscore the similarities in energies for the μ-perpendicular, parallel, and skewed geometries and that of the η^2-isomer. Given the similarities of the fragments d^2-W$(OR)_4$ and d^8-OsL_4, we can speculate that for certain combinations of neutral ligands L, Os_2L_8(alkyne) complexes will be found to adopt a related η^2-alkyne structure.

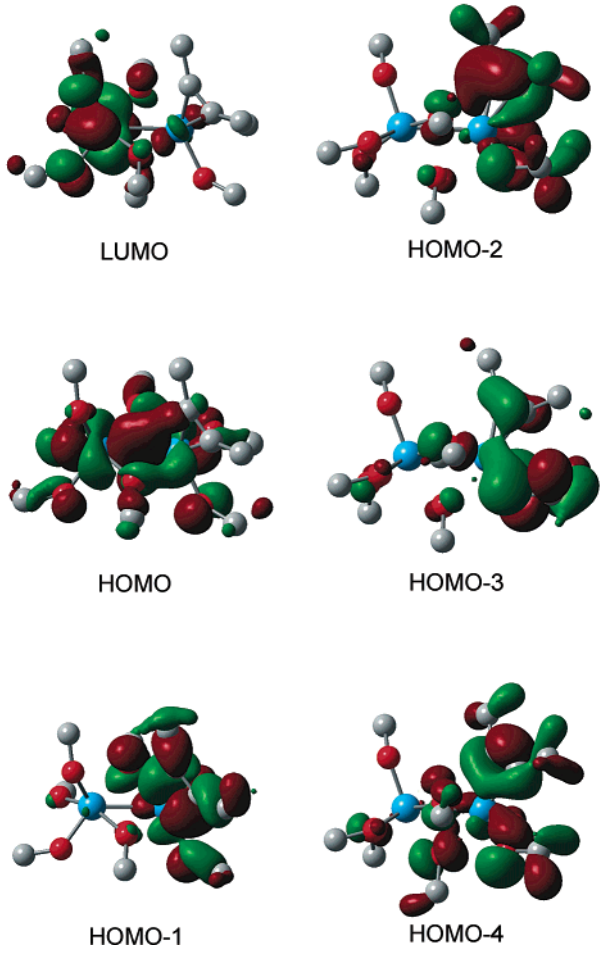

Figure 10. Selected DFT [B3LYP(SDD,6-31G*)] calculated Gaussview[20] plots of the frontier molecular orbitals of $W_2(\eta^2\text{-MeC}{\equiv}\text{CMe})(\mu\text{-OCH}_3)_3(\text{OCH}_3)_5$.

Experimental Section

All manipulations were carried out under an inert atmosphere of oxygen-free UHP-grade argon using standard Schlenk techniques or under a dry and oxygen-free atmosphere of nitrogen in a Vacuum Atmospheres dry lab system. Hexane was degassed and distilled from potassium under nitrogen. Toluene was degassed and distilled from sodium under nitro-

gen. Et_2O was degassed and distilled from sodium benzophenone ketyl under nitrogen. Toluene-d_8 was degassed, stirred over sodium for 24 h, and vacuum transferred to an ampoule. Phenylpropyne, phenylacetylene, trimethylsilylacetylene, and 2-butyne were purchased from Aldrich, degassed, and dried over 4Å sieves for 24 h prior to use. Propyne was purchased from Pfaltz & Bauer and used as received. $[W_2(OCH_2{}^tBu)_8]_n$ was prepared according to literature procedures.[21]

NMR spectra were recorded on 400 MHz Bruker DPX Avance^{400} or 600 MHz Bruker spectrometers. All ^{1}H NMR chemical shifts are reported in ppm relative to the ^{1}H impurity in toluene-d_8 at δ 2.09. IR spectra were recorded as Nujol mulls using KCl windows on a Perkin-Elmer Spectrum GX spectrometer. Mass spectra were obtained on a Kratos MS-890 mass spectrometer under electron impact ionization conditions.

Preparation of $W_2(\mu\text{-}OCH_2{}^tBu)_2(\mu\text{-}\eta^2,\eta^2\text{-}PhC{\equiv}CH)(OCH_2{}^tBu)_6$. To a 25 mL round-bottomed flask was added $[W_2(ONp)_8]_n$ (0.100 g, 0.094 mmol). Hexanes (10 mL) were added to give a purple slurry. PhC≡CH (10.3 μL, 0.094 mmol) was added by syringe to give a clear green solution. After stirring 8 h, the solution was filtered through a medium glass frit with a Celite pad. Evaporation of the solvent gave a green solid identified as $W_2(\mu\text{-}OCH_2{}^tBu)_2(\mu\text{-}\eta^2,\eta^2\text{-}PhC{\equiv}CH)(OCH_2{}^tBu)_6$ in 95% yield. X-ray quality crystals were obtained upon crystallization from Et_2O at −20 °C. ^{1}H NMR (400 MHz, toluene-d_8, 115 °C): δ 0.95 (s, 72 H), 4.57 (s, 16 H), 7−8 (m, Ph), 12.09 (s, 1 H, $^2J_{W-H}$ = 8 Hz (25%)). ^{1}H NMR (400 MHz, toluene-d_8, −30 °C): δ 0.70 (s, 18 H), 0.99 (s, 18 H), 1.09 (s, 9 H), 1.23 (s, 9 H), 1.27 (s, 18 H), 4.18 (d, 2 H, J_{H-H} = 11.6 Hz), 4.45 (d, 2 H, J_{H-H} = 12 Hz), 4.50 (d, 2 H, 11.6 Hz), 4.66 (s, 2 H), 4.63 (multiplet of overlapping dublets, 6 H), 5.26 (s, 2 H), 12.09 (s, 1 H, $^2J_{W-H}$ = 8 Hz (25%)). ^{13}C{^{1}H} NMR (100 MHz, toluene-d_8, 115 °C): δ 26.58 (s, *C*H$_3$), 33.14 (s, *C*H$_2$) 84.00 (s, *C*(CH$_3$)$_3$, 120−140 (m, Ph), 176.22 (s, PhC≡*C*H), 210.29 (s, Ph*C*≡CH). ^{13}C{^{1}H} NMR (150 MHz, toluene-d_8, 25 °C, alkyne region): δ 174. 40 (s, PhC≡*C*H, J_{W-C} = 22 Hz, (25%)), 212.33 (s, Ph*C*≡CH, J_{W-C} = 20 Hz (25%)). Anal. Calcd for $W_2O_8C_{48}H_{94}$: C, 49.40; H, 8.13. Found: C, 49.82; H, 7.91.

Preparation of $W_2(\mu\text{-}OCH_2{}^tBu)_3(\eta^2\text{-}TMSC{\equiv}CH)(OCH_2{}^tBu)_5$. To a 25 mL round-bottomed flask was added $[W_2(ONp)_8]_n$ (0.100 g, 0.094 mmol). Hexanes (10 mL) were added to give a purple slurry. TMSC≡CH (15 μL, 0.094 mmol) was added by syringe, and the reaction mixture was heated to 45 °C. Slowly, over 3 h the purple slurry changed to a clear green solution. The solution was further stirred 3 h. Filtration through a medium glass frit with a Celite pad gave a green solid identified as $W_2(\mu\text{-}OCH_2{}^tBu)_3(\eta^2\text{-}TMSC{\equiv}CH)(OCH_2{}^tBu)_5$ in 95% yield. ^{1}H NMR (400 MHz, toluene-d_8, 40 °C): δ 0.47 (s, 9 H), 0.79 (s, 9 H), 0.94 (s, 9 H), 1.10 (s, 18 H), 1.11 (s, 18 H), 1.15 (s, 18 H), 4.00 (s, 2 H), 4.10, (s, 2 H), 4.51 (d, 2 H, J_{H-H} = 10.4 Hz), 4.58 (d, 2 H, J_{H-H} = 11.2 Hz), 4.66 (d, 2 H, J_{H-H} = 11.2 Hz), 4.89 (d, 2 H, J_{H-H} = 11.6 Hz), 4.93 (d, 2 H, J_{H-H} = 11.2 Hz), 4.94 (d, 2 H, J_{H-H} = 10.8 Hz), 12.94 (1 H, $^2J_{W-H}$ = 10 Hz (12.5%)). ^{13}C{^{1}H} NMR (100 MHz, toluene-d_8, 40 °C): δ 2.40 (s, Si*C*H$_3$) 26.37 (s, *C*H$_3$), 27.75 (s, *C*H$_3$), 27.82 (s, *C*H$_3$), 27.94 (s, *C*H$_3$), 28.49 (s, *C*H$_3$), 33.41 (s, *C*H$_2$), 33.88 (s, *C*H$_2$), 34.80 (s, *C*H$_2$), 35.49 (s, *C*H$_2$), 35.67 (s, *C*H$_2$) 73.72 (s, *C*(CH$_3$)$_3$, 76.26 (s, *C*(CH$_3$)$_3$, 85.12 (s, *C*(CH$_3$)$_3$, 87.21 (s, *C*(CH$_3$)$_3$, 87.84 (s, *C*(CH$_3$)$_3$, 204.52 (TMS*C*≡CH, $J^{183}{}_{W-^{13}C}$ = 48 Hz), 222.83 (TMSC≡*C*H, $J_{W-^{13}C}$ = 43 Hz). NOE spectra were used to establish exchange of alkoxide groups. IR (ν_{max}/cm^{-1}): 1558 (w), 1548 (w), 1479 (s), 1462 (s), 1391 (s), 1377 (m), 1361 (s), 1289 (vw), 1260 (w), 1245 (w), 1214 (w), 1110 (m), 1085 (s), 1058 (s), 1046 (s), 1034 (s), 1022 (s), 1009 (s), 967 (vw), 934 (vw), 901 (vw), 861 (s), 838 (m), 805 (w), 758 (w), 753 (w), 722 (vw), 676 (s), 650 (m), 637 (s), 614 (w), 592 (vw), 460 (w), 407 (w), 383 (w), 377 (w), 375 (m). Anal. Calcd for $W_2O_8C_{45}SiH_{97}$: C, 46.46; H, 8.50. Found: C, 45.41; H, 8.65.

Preparation of $W_2(OCH_2{}^tBu)_8(MeC{\equiv}CMe)$. To a 25 mL round-bottomed flask was added $[W_2(ONp)_8]_n$ (0.100 g, 0.094 mmol). Hexanes (10 mL) were added to give a purple slurry. MeCCMe (8 μL, 0.094 mmol) was added by syringe, and the purple slurry changed to a clear green solution. The reaction was further stirred 3 h. Filtration through a medium glass frit with a Celite pad followed by evaporation of the solvent gave a green solid. ^{1}H NMR spectra in toluene-d_8 revealed a mixture of two isomers $W_2(\mu\text{-}OCH_2{}^tBu)_2(\mu\text{-}\eta^2,\eta^2\text{-}MeC{\equiv}CMe)(OCH_2{}^tBu)_6$ (isomer **A**) and $W_2(\mu\text{-}OCH_2{}^tBu)_3(\eta^2\text{-}MeC{\equiv}CMe)(OCH_2{}^tBu)_5$ (isomer **B**) in a 1:9 ratio, respectively. X-ray quality crystals of $W_2(\mu\text{-}OCH_2{}^tBu)_2(\mu\text{-}\eta^2,\eta^2\text{-}MeC{\equiv}CMe)(OCH_2{}^tBu)_6$ (**A**) (the minor isomer present in solution) were obtained by low-temperature crystallization from Et_2O. ^{1}H NMR (400 MHz, 25 °C, toluene-d_8) of isomer **A**: δ 1.06 (s, 72 H), 3.20 (s, 6 H), 4.57 (s, 16 H). ^{13}C{^{1}H} NMR (100 MHz, −50 °C, toluene-d_8) of isomer **A**: δ 28.43 (s, *C*H$_3$), 35.45 (s, *C*H$_2$), 83.46 (s, *C*(CH$_3$)), alkyne carbons not detected. ^{1}H NMR (400 MHz, 25 °C, toluene-d_8) of isomer **B**: δ 0.81 (s, 9 H), 0.95 (s, 9 H), 1.10 (s, 18 H), 1.16 (s, 18 H), 1.17 (s, 18 H), 2.92 [(s, MeC≡CMe, 6 H) at −40 °C there are two singlets: 2.89, 3 H and 2.96, 3 H], 3.94 (s, 2 H), 4.06 (s, 2 H), 4.52 (d, 2 H, J_{H-H} = 11.0 Hz), 4.59 (d, 2 H, J_{H-H} = 10.7 Hz), 4.65 (d, 2 H, J_{H-H} = 11.1 Hz), 4.80 (d, 2 H, J_{H-H} = 10.6 Hz), 4.86 (d, 2 H, J_{H-H} = 11.1 Hz), 5.01 (d, 2 H, J_{H-H} = 11.0 Hz). ^{13}C{^{1}H} NMR (100 MHz, −50 °C, toluene-d_8) of isomer **B**: δ 25.96 (s, MeC≡CMe), 26.10 (s *C*H$_3$), 26.52 (s, MeC≡CMe), 27.44 (s, *C*H$_3$), 27.54 (s, *C*H$_3$), 27.58 (s, *C*H$_3$), 28.23 (s, *C*H$_3$), 33.30 (s, *C*H$_2$), 33.74 (s, *C*H$_2$), 34.30 (s, *C*H$_2$), 35.11 (s, *C*H$_2$), 35.31 (s, *C*H$_2$), 73.27 (s, *C*(CH$_3$)$_3$), 73.68 (s, *C*(CH$_3$)$_3$), 85.36 (s, *C*(CH$_3$)$_3$), 85.73 (s, *C*(CH$_3$)$_3$), 88.65 (s, *C*(CH$_3$)$_3$), 196.85 (MeC≡CMe), 210.46 (MeC≡CMe). ^{13}C{^{1}H} NMR (100 MHz, 80 °C, toluene-d_8) of isomer **B**: δ 27.31 (s, *C*H$_3$), 27.84 (s, MeCCMe), 28.21 (s, *C*H$_3$), 28.39 (s, *C*H$_3$), 28.49 (s, *C*H$_3$), 29.20 (s, *C*H$_3$), 34.27 (s, *C*H$_2$), 34.91 (s, *C*H$_2$), 35.11 (s, *C*H$_2$), 35.67 (s, *C*H$_2$), 35.83 (s, *C*H$_2$), 75.94 (s, *C*(CH$_3$)), 76.23 (s, *C*(CH$_3$)), 85.99 (s, *C*(CH$_3$)), 87.01 (s, *C*(CH$_3$)), 89.29 (s, *C*(CH$_3$)), alkyne carbons not detected. Anal. Calcd for $W_2O_8C_{44}H_{94}$: C, 47.23; H, 8.47. Found: C, 47.24; H, 8.38.

Preparation of $W_2(\mu\text{-}OCH_2{}^tBu)_3(\eta^2\text{-}PhC{\equiv}CMe)(OCH_2{}^tBu)_5$. To a 25 mL round-bottomed flask was added $[W_2(ONp)_8]_n$ (0.100 g, 0.094 mmol). Hexanes (10 mL) were added to give a purple slurry. PhC≡CMe (11 μL, 0.094 mmol) was added by syringe, and the purple slurry changed to a clear green solution. The reaction was further stirred 3 h. Filtration through a medium glass frit with a Celite pad followed by stripping the solvent gave a green solid. ^{1}H NMR spectra in toluene-d_8 revealed a mixture of two isomers $W_2(\mu\text{-}OCH_2{}^tBu)_2(\mu\text{-}\eta^2,\eta^2\text{-}PhC{\equiv}CMe)(OCH_2{}^tBu)_6$ (isomer **A**) and $W_2(\mu\text{-}OCH_2{}^tBu)_3(\eta^2\text{-}PhC{\equiv}CMe)(OCH_2{}^tBu)_5$ (isomer **B**) in a 1:3 ratio, respectively, by ^{1}H NMR. Single crystals of $W_2(\mu\text{-}OCH_2{}^tBu)_3(\eta^2\text{-}PhC{\equiv}CMe)(OCH_2{}^tBu)_5$ (**B**) were obtained by slow evaporation of a toluene solution in an NMR tube in a nitrogen atmosphere glovebox. ^{1}H NMR (400 MHz, 25 °C, toluene-d_8) of isomer **A**: δ 1.01 (br s, 72 H), 3.61 (s, 3H), 4.51 (br s 16 H), 7−8 (m, Ph). ^{13}C{^{1}H} NMR (100 MHz, 27 °C, toluene-d_8) of isomer **A**: δ 23.08 (s, *Me*C≡CPh), 27.53 (br s, *C*H$_3$), 33.63 (br s, *C*H$_2$), 87.15 (s, *C*(CH$_3$)), 120−140 (s, *Ph*). ^{13}C{^{1}H} NMR (150 MHz, 60 °C, toluene-d_8) of isomer **A**: δ 202.46 (s, MeC≡CPh), 215.18 (MeC≡*C*Ph). ^{1}H NMR (400 MHz, 25 °C, toluene-d_8) of isomer **B**: δ 0.84 (s, 9 H), 0.95 (s, 9 H), 1.09 (s, 18 H), 1.16 (s, 18 H), 1.17 (s, 18 H), 3.07 (s, 6 H), 3.99 (s, 2 H), 4.09 (s, 2 H), 4.61 (d, 2 H, J_{H-H} = 10.9 Hz), 4.70 (d, 2 H, J_{H-H} = 11.5 Hz), 4.79 (d, 2 H, J_{H-H} = 10.9 Hz), 4.88 (d, 2 H, J_{H-H} = 10.8 Hz), 4.91 (d, 2 H, J_{H-H} = 10.9 Hz), 5.06 (d, 2 H, J_{H-H} = 11.0 Hz), 7−8 (m, Ph). ^{13}C{^{1}H} NMR (100 MHz, 27 °C, toluene-d_8) of isomer **B**: δ 21.54 (s, PhC≡C*C*H$_3$) 26.56 (s, *C*H$_3$), 27.72 (s, *C*H$_3$), 27.74 (s, *C*H$_3$), 27.72 (s, *C*H$_3$) 28.65 (s, *C*H$_3$), 32.03 (s, *C*H$_2$), 33.57 (s, *C*H$_2$), 33.67 (s, *C*H$_2$), 34.31 (s, *C*H$_2$), 35.21 (s, *C*H$_2$), 74.73 (s, *C*(CH$_3$), 75.01 (s, *C*(CH$_3$), 85.58 (s, *C*(CH$_3$), 86.76

(20) *GaussView 2.1*; Gaussian Inc.: Pittsburgh, PA, 1998.
(21) Budziochowski, T. A.; Chisholm, M. H.; Folting, K.; Huffman, J. C.; Streib, W. E. *J. Am. Chem. Soc.* **1995**, *117*, 7428.

Table 6. Crystallographic Details for $W_2(\mu\text{-}\eta^2,\eta^2\text{-PhC}{\equiv}\text{CH})(\mu\text{-OCH}_2{}^t\text{Bu})_2(\text{OCH}_2{}^t\text{Bu})_6$ (1), $W_2(\mu\text{-}\eta^2,\eta^2\text{-MeC}{\equiv}\text{CMe})(\mu\text{-OCH}_2{}^t\text{Bu})_2(\text{OCH}_2{}^t\text{Bu})_6$ (2), $W_2(\mu\text{-}\eta^2,\eta^2\text{-MeC}{\equiv}\text{CH}))(\mu\text{-OCH}_2{}^t\text{Bu})_2(\text{OCH}_2{}^t\text{Bu})_6$ (3), and $W_2(\eta^2\text{-PhC}{\equiv}\text{CMe})(\mu\text{-OCH}_2{}^t\text{Bu})_3(\text{OCH}_2{}^t\text{Bu})_5$ (4)

	1	2	3	4
empirical formula	$C_{48}H_{94}O_8W_2$	$C_{44}H_{94}O_8W_2$	$C_{43}H_{92}O_8W_2$	$C_{49}H_{96}O_8W_2$
fw	1166.93	1118.89	1104.87	1180.96
temperature	200(2) K	150(2) K	200(2) K	150(2) K
wavelength	0.71073 Å	0.71073 Å	0.71073 Å	0.71073 Å
space group	$P2_1/n$	$C2/c$	$P2_1/c$	$P2_1/c$
unit cell dimens	a = 13.788(1)Å b = 16.743(1)Å c = 23.934(2) Å β = 93.02(1)°	a = 25.524(2) Å b = 10.022(1) Å c = 21.593(2) Å β = 110.04(1)°	a = 23.623(3)Å b = 11.917(1)Å c = 18.813(2)Å β = 100.12(1)°	a = 13.702(2) Å b = 19.356(3) Å c = 21.128(4) Å β = 103.29(1)°
volume	5517.6(7) Å^3	5189.1(9) Å^3	5214(1) Å^3	5453(2) Å^3
Z	4	4	4	4
density (calcd)	1.405 Mg/m^3	1.432 Mg/m^3	1.408 Mg/m^3	1.438 Mg/m^3
abs coeff	4.210 mm^{-1}	4.473 mm^{-1}	4.451 mm^{-1}	4.260 mm^{-1}
cryst size	0.08 × 0.12 × 0.27 mm	0.04 × 0.08 × 0.38 mm	0.08 × 0.08 × 0.23 mm	0.19 × 0.08 × 0.04 mm
θ range	2.43 to 27.49°	2.14 to 27.48°	2.13 to 27.47°	2.10 to 25.08°
no. of reflns collected	95 513	55 154	82 490	52 119
no. of indep reflns	12 638 [R(int) = 0.060]	5942 [R(int) = 0.078]	11 936 [R(int) = 0.051]	9505 [R(int) = 0.089]
no. of data/restraints/params	12 638/0/547	5942/0/257	11 936/0/507	9504/0/558
goodness-of-fit on F^2	1.011	1.040	1.032	1.033
final R indices [$I>2\sigma(I)$][a]	R1 = 0.0301, wR2 = 0.0541	R1 = 0.0264, wR2 = 0.0460	R1 = 0.0271, wR2 = 0.0442	R1 = 0.0510, wR2 = 0.0951
R indices (all data)	R1 = 0.0671, wR2 = 0.0616	R1 = 0.0462, wR2 = 0.0498	R1 = 0.0449, wR2 = 0.0474	R1 = 0.1047, wR2 = 0.1142
largest diff peak and hole	1.56 and −1.07 e/A^3	1.23 and −1.21 e/Å^3	1.31 and −0.55 e/Å^3	2.44 and −1.24 e/Å^3

[a] $R1 = \sum||F_o| - |F_c||/\sum|F_o|$ and $wR2 = [\sum w(F_o^2 - F_c^2)^2/\sum w(F_o^2)^2]^{1/2}$.

(s, *C*(CH$_3$), 89.38 (s, *C*(CH$_3$), 120−140 (s, *Ph*), 192.46 (s, PhC≡*C*Me, J_{W-C} = 24 Hz), 209.75 (br s, Ph*C*≡CMe,).^{13}C{^{1}H} NMR (150 MHz, 60 °C, toluene-d_8) of isomer **B**: δ 192.46 (s, PhC≡*C*Me, J_{W-C} = 24 Hz), 209.75 (s, Ph*C*≡CMe, J_{W-C} = 29 Hz). Anal. Calcd for $W_2O_8C_{49}H_{96}$: C, 49.83; H, 8.19. Found: C, 49.82; H, 7.91.

Preparation of $W_2(\mu\text{-OCH}_2{}^t\text{Bu})_2(\mu\text{-}\eta^2,\eta^2\text{-MeC}{\equiv}\text{CH})(\text{OCH}_2{}^t\text{Bu})_6$. To a 25 mL round-bottomed flask was added $[W_2(\text{ONp})_8]_n$ (0.100 g, 0.094 mmol). Hexanes (10 mL) were added to give a purple slurry. MeC≡CH (0.094 mmol) was added via a calibrated gas addition manifold at −196°. Upon warming, the purple slurry changed to a clear green solution. The reaction was further stirred 3 h. Filtration through a medium glass frit with a Celite pad followed by stripping the solvent gave a reddish-brown solid. ^{1}H NMR spectra in toluene-d_8 revealed a mixture of two isomers of $W_2(\mu\text{-OCH}_2{}^t\text{Bu})_2(\mu\text{-}\eta^2,\eta^2\text{-MeC}{\equiv}\text{CH})(\text{OCH}_2{}^t\text{Bu})_6$ (isomer **A**) and $W_2(\mu\text{-OCH}_2{}^t\text{Bu})_3(\eta^2\text{-MeC}{\equiv}\text{CH})(\text{OCH}_2{}^t\text{Bu})_5$ (isomer **B**) in a 3:1 ratio, respectively. ^{1}H NMR (400 MHz, 25 °C, toluene-d_8) of isomer **A**: δ 0.84 (br s, 72 H), 2.95 (d, $^4J_{H-H}$ = 1.2 Hz), 4.37 (br s, 16 H), 11.71 (q, 1 H, $^2J_{W-H}$ = 9.6 Hz (25%)). ^{13}C{^{1}H} NMR (100 MHz, 27 °C, toluene-d_8) of isomer **A**: δ 26.42 (*Me*CCH), 28.09 (br s, *C*H$_3$), 35.05 (br s, *C*H$_2$), 68.29 (s, *C*(CH$_3$)$_3$, 177.68 (s, J_{W-C} = 22 Hz), 220.93 (s, J_{W-C} = 20 Hz). ^{1}H NMR (400 MHz, 25 °C, toluene-d_8) of isomer **B**: δ 0.62 (s, 9 H), 0.76 (s, 9 H), 0.90 (s, 18 H), 0.96 (s, 18 H), 0.98 (s, 18 H), 3.22 (d, 3 H, $^4J_{H-H}$ = 1.2 Hz), 3.78 (s, 2 H), 3.88 (s, 2 H), 4.34 (d, 2 H, J_{H-H} = 10.4 Hz), 4.41 (d, 2 H, J_{H-H} = 10.8 Hz), 4.49 (d, 2 H, J_{H-H} = 10.8 Hz), 4.61 (d, 2 H, J_{H-H} = 10.4 Hz), 4.71 (d, 2 H, J_{H-H} = 11.2 Hz), 4.76 (d, 2 H, J_{H-H} = 11.2 Hz), 11.47 (q, 1 H, $^2J_{W-H}$ = 10.4 Hz, (12.5%)). ^{13}C{^{1}H} NMR (100 MHz, 27 °C, toluene-d_8) of isomer **B**: δ 22.73 (*Me*CCH), 27.10 (s, *C*H$_3$), 28.31 (s, *C*H$_3$), 28.38 (s, *C*H$_3$), 28.42 (s, *C*H$_3$), 29.03 (s, *C*H$_3$), 34.05 (s, *C*H$_2$), 34.42 (s, *C*H$_2$), 34.98 (s, *C*H$_2$), 35.74 (s, *C*H$_2$), 35.89 (s, *C*H$_2$), 75.01 (s, *C*(CH$_3$), 76.56 (s, *C*(CH$_3$), 85.74 (s, *C*(CH$_3$), 87.00 (s, *C*(CH$_3$), 88.03 (s, *C*(CH$_3$), 199.65 (s, MeCCH), 203.45 (s, MeCCH). Anal. Calcd for $W_2O_8C_{43}H_{92}$: C, 46.75; H, 8.39. Found: C, 46.62; H, 8.27. MS(EI): calcd for 1104.58; found *m*/*z* 1104.88.

Electronic Structure Calculations. Density functional theory (DFT)[12,13] calculations with the Gaussian 98 suite of programs[14] utilized the B3LYP[15−17] method and standard basis sets. C, H, O, and Si were described with the 6-31G* basis set[18] (and five "pure" d functions), while W was represented by an SDD effective core potential.[19] The geometries were optimized under C_1 symmetry starting from the solid-state structure coordinates using the default optimization criteria. The neopentoxide ligands were replaced by methoxides. Single-point energy calculations were carried out for μ-perpendicular and parallel alkyne adducts, and calculations were started with μ-skewed geometries θ = 45° and allowed to optimize. All stationary points were characterized as minima by vibrational frequency calculations.

Crystallographic Studies. Crystallographic details for the four structures are presented in Table 6. All data sets were measured on a Nonius Kappa CCD diffractometer equipped with an Oxford Cryosystems cryostream cooler. A combination of phi and omega scans with a frame width of 1.0° was used for all four structures. Data integration was done with Denzo.[22] Full details are given in the Supporting Information.

Crystal structure data have also been deposited with the Cambridge Crystallographic Data Center: Structure #1 is CCDC No. 188146, Structure #2 is CCDC No. 187844, Structure #3 is CCDC No. 192251 and Structure #4 is CCDC No. 187843.

Acknowledgment. We thank the National Science Foundation for support and the Ohio Supercomputing Center for computational resources.

Supporting Information Available: Full details of structural determinations. This material is available free of charge via the Internet at http://pubs.acs.org.

OM030498O

(22) *DENZO*: Otwinowski, Z.; Minor, W. *Methods in Enzymology*, Vol 276: *Macromolecular Crystallography*; Carter, Jr., C. W., Sweet, R. M., Eds.; Academic Press: New York, 1997; Part A, pp 307−326.
(23) *teXsan*: Crystal Structure Analysis Package, version 1.7-2; Molecular Structure Corporation: The Woodlands, TX, 1995.
(24) *SHELXS-86*: Sheldrick, G. M. *Acta Crystallogr.* **1990**, *A46*, 467−473.
(25) Sheldrick, G. M. *SHELXL-93*; Universitat Gottingen, Germany, 1993.
(26) *International Tables for Crystallography*; Kluwer Academic Publishers: Dordrecht, 1992; Vol. C.
(27) *SORTAV*: Blessing, R. H. *Acta Crystallogr.* **1995**, *A51*, 33−37. Blessing, R. H. *J Appl. Crystallogr.* **1997**, *30*, 421−426.
(28) Sheldrick, G. M. *SHELXL-97*; Universitat Gottingen: Germany, 1997.
(29) Sheldrick, G. M. *SHELXS-97*; Universitat Gottingen: Germany, 1997.